

## SUB-PIXEL EDGE LOCALIZATION BASED ON LASER WAVEFORM ANALYSIS

B. Jutzi<sup>a</sup>, J. Neulist<sup>a</sup>, U. Stilla<sup>b</sup>

<sup>a</sup> FGAN-FOM Research Institute for Optronics and Pattern Recognition, 76275 Ettlingen, Germany - {jutzi,neulist}@fom.fgan.de

<sup>b</sup> Photogrammetry and Remote Sensing, Technische Universitaet Muenchen, 80290 Muenchen, Germany - stilla@bv.tum.de

### Commission III, Working Group III/3

**KEY WORDS:** Urban, Analysis, Laser scanning, LIDAR, Edge, Sub-pixel precision.

#### ABSTRACT:

Laser range data is of high interest in photogrammetry. However, compared to passive imagery, it usually has a lower image resolution, making geometry extraction and modeling challenging. A method to overcome this handicap using a laser scanner capable of full waveform analysis is proposed. The recorded pulse waveform is analyzed to find range and intensity values for all of the surfaces in the beam footprint. Sub-pixel edge localization is implemented and tested for straight edges of man-made objects, allowing a much higher precision of geometry extraction in urban areas. The results show that it is possible to find edges with an accuracy of at least one tenth of a pixel.

#### 1. INTRODUCTION

The automatic generation of 3-d models for a description of man-made objects, like buildings, is of great interest in photogrammetric research. In photogrammetry, a spatial surface is classically measured by triangulation of corresponding image points from two or more pictures of the surface. The points are manually chosen or automatically detected by analyzing image structures. Besides this indirect measurement using object characteristics dependant on natural illumination, active laser scanner systems allow a direct and illumination-independent measurement of range. Laser scanners capture the range of 3-d objects in a fast, contactless and accurate way. Overviews for laser scanning systems are given in (Huising & Pereira, 1998; Wehr & Lohr, 1999; Baltsavias, 1999).

For the task of automatic model generation, a precise measurement of the edges and vertices of regularly shaped objects is paramount. Often, the spatial resolution of laser scanners used in urban surveying is not sufficient for this. In this case, an approach to locate the edges with sub-pixel accuracy is desirable. To achieve this, as much information as possible should be gained per pixel<sup>1</sup> to offset the low number of pixels in the image.

Current pulsed laser scanner systems for topographic mapping are based on time-of-flight ranging techniques to determine the range of the illuminated object. The signal analysis to determine the elapsed time between the emitted and backscattered laser pulses typically operates by analogous threshold detection. Some systems capture multiple reflections caused by objects which are smaller than the footprint located in different ranges. Such systems usually record the first and the last backscattered laser pulse (Baltsavias, 1999).

First pulse as well as last pulse exploitation is used for different applications like urban planning or forestry surveying. While first pulse registration is the optimum choice to measure the hull of partially penetrable objects (e.g. canopy of trees), last pulse registration should be chosen to measure non-penetrable surfaces (e.g. ground surface). Due to multiple pulse reflection at the boundary of buildings and the processing by first or last

pulse mode, building areas dilate or erode. For visualizing the various sizes of the building footprints in first and last pulse images a difference image can be calculated. The actual building edges are then expected within the bright areas in this image (Figure 1).

Apart from the range measurement of laser scanner systems some systems deliver a single reflectance value derived from the intensity or the power of the backscattered laser light. The intensity is determined by the signal maximum and the power by signal integration of the measured laser light and gives radiometric information about the surveyed area. This intensity (power) value can be used for separating segments of artificial objects from vegetation (Hug & Wehr, 1997; Maas, 2001).

One step further, the complete waveform of the recorded signal might be of interest, because it includes the backscattering characteristic of the illuminated field. Investigations on analyzing the waveform were done to explore the vegetation concerning the bio mass, foliage or density (e.g. trees, bushes, and ground). Recent laser scanner system developments provide commercial airborne laser scanning systems that allow capturing the waveform: RIEGL LMS-Q560, LITEMAPPER 5600, OPTECH ALTM 3100, TOPEYE II. To interpret the backscattered waveform, a better understanding of the physical principles is important and has to be developed. The physical measurement process and the influence of the surface on the emitted waveform are discussed by (Jutzi & Stilla, 2002; Wagner *et al.*, 2004).

By analyzing the backscattered waveform for the received pulses it is possible to determine specific surface properties for each received pulse. Typical surface properties of interest can be distance, roughness, reflectance and number of surface responses. The estimates of these properties can be used for further processing. Vosselman (2002) suggested considering the reflectance strength of the laser beam response to estimate and improve the accuracy of reflectance edge positions. Besides the edge positions of planimetric offsets, the estimation of edges in different heights is investigated by considering the reflectance strength to increase the accuracy of boundaries at plane surfaces, where the height data captured with laser scanner systems generally suffers by unresolved ambiguity.

In this paper we describe investigations for a detailed analysis of laser pulses. In Section 2, our method for generation of

<sup>1</sup> Note that in this paper the label *pixel* describes the conical region in space illuminated by a single laser beam. During visualization, this region is compressed into a single pixel of a displayed image, hence the name.

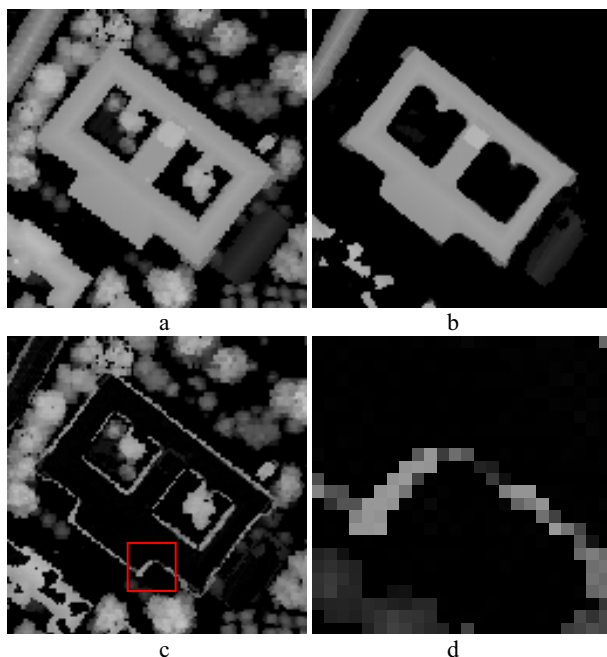


Figure 1. Sections of an urban scene (Test area Karlsruhe, Germany).

- a) elevation images captured by first pulse mode,
- b) elevation images captured by last pulse mode,
- c) difference image of first and last pulse mode,
- d) section of the difference image (building boundary).

synthetic test data is discussed. A description of the general waveform analysis, image segmentation and surface boundary extraction can be found in Section 3. The actual sub-pixel edge localization algorithms are developed in Section 4. Section 5 presents results and a discussion of the merits and flaws of the method.

## 2. DATA GENERATION

To simulate the temporal waveform of the backscattered pulses a *scene model* (i) and a *sensor model* (ii) is required (Jutzi & Stilla, 2004).

### 2.1 Scene modeling

#### 2.1.1 Scene representation

For a 3-d scene representation, our simulation setup considers geometric and radiometric features of the illuminated surface in the form of a 3-d object model with homogeneous surface reflectance.

#### 2.1.2 Sampling

The object model with homogeneous surface reflectance is then sampled at a higher spatial resolution than the scanning grid we simulate and process, to enable us to simulate the spatial distribution of the laser beam. Considering the position and orientation of the sensor system we receive high-resolution range and intensity images (45-fold oversampling, i.e. one image pixel is produced by averaging over 45x45 high-resolution sub-pixels. The oversampling window size does not have any practical relevance if it is sufficiently large to not induce errors in a higher magnitude as those incurred by our discretized beam profile). Depending on the predetermined position and orientation of the sensor system, various range images can be captured.

### 2.2 Sensor modeling

The sensor modeling takes into account the specific properties of the sensing process: the position and orientation of the sensor, the laser pulse description, scanning and the receiver properties.

#### 2.2.1 Orientation

To simulate varying perspectives, a description of the extrinsic orientation of the laser scanning system with the help of a GPS/INS system is used.

#### 2.2.2 Laser pulse description

The transmitted laser pulse of the system is characterized by specific pulse properties (Jutzi et al., 2002). We assume a Gaussian pulse energy distribution in both space and time, the spatial distribution thus being radially symmetric. With real data, the sampled actual pulse distribution depending on the used laser type can be used to model the edge appearance in the image (q.v. Section 4.1).

#### 2.2.3 Scanning

Depending on the scan pattern of the laser scanner system, the grid spacing of the scanning, and the divergence of the laser beam, a sub-area of the high-resolution range image is processed. By convolving this sub-area with the temporal waveform of the laser pulse, we receive a high-resolution intensity cube. Furthermore, the corresponding sub-area of the high-resolution intensity image is weighted with the spatial energy distribution of the laser beam, where the grid spacing is taken to be  $6\sigma$  of the spatial beam energy distribution (i.e. the grid lines are at  $\pm 3\sigma$  relative to the beam center) to take into account the amount of backscattered laser light for each reflectance value. Then we have a description of the backscattered laser beam with a higher spatial resolution than necessary for processing.

#### 2.2.4 Receiver

By focusing the beam with its specific properties on the detector of the receiver, the spatial resolution is reduced and this is simulated with a spatial undersampling of the sub-areas.

Finally we receive an intensity cube spaced with the scanning width of the simulated laser scanner system and containing the temporal description of the backscattered signal. Because each intensity value in the sub-area is processed by undersampling, multiple reflections can be observed in the backscattered signal.

## 3. DATA ANALYSIS

Algorithms are developed and evaluated with simulated signals of synthetic objects. First, a signal preprocessing of the intensity cube with a matched filter is implemented to improve the detection rate. These results are used to analyze the waveform of each pulse for gaining the surface properties: range, reflectance and number of peaks. Then the surface properties are processed with a region based segmentation algorithm. By the use of images the region boundary pixels derived from multiple reflections at the same spatial position are shared by separate regions.

### 3.1 Pulse property extraction

Depending on the size of the observed surface geometry in relation to the laser beam (footprint and wavelength) different properties can be extracted (Jutzi & Stilla, 2003). In this paper we focus on the pulse properties average time value, maximum intensity and number of peaks.

- The average time value is processed to determine the distance from the system to the illuminated surface.
- The maximum intensity value is computed to get a description for the reflectance strength of the illuminated area.
- Multiple peaks in one signal indicate multiple surfaces at differing ranges illuminated by the beam. Therefore, they are clues to object boundaries.

For determining the property values for each pulse of the whole waveform the intensity cube is processed in different ways. First, the pulse has to be detected in the signal profile by using a matched filter. Then, a neighborhood area of interest in the temporal waveform is selected for temporal signal analysis.

For obtaining surface characteristics, each waveform of the cube is analyzed for pulse property values. For pulse detection it is necessary to separate each single pulse from the background noise. The number of detected pulses depends critically on this separation method. Therefore the signal background noise is estimated, and where the intensity of the waveform is above three times the noise standard deviation for a duration of at least 5 ns (full-width-half-maximum of the pulse), a pulse is assumed to have been found and a waveform interval including the pulse is accepted for further processing.

Typical surface features we wish to extract from a waveform are *range*, *roughness*, and *reflectance*. The corresponding pulse properties of these surface features are: *time*, *width* and *intensity*. Because of the strong fluctuations of the waveform, extracting the relevant properties of the waveform can be difficult. Therefore, the recorded waveform is approximated by a Gaussian to get a parametric description. Fitting a Gaussian to the complete waveform instead of quantizing a single value of the waveform has the advantage of decreasing the influence of noise and fluctuation. To solve the Gaussian mixture problem, the Gauss-Newton method (Hartley & Zisserman, 2000) with iterative parameter estimation is used. The estimated parameters for pulse properties are the averaged time value  $\tau$ , standard deviation  $\sigma$  and maximum intensity  $a$ :

$$w(t - \tau) = \frac{a}{\sqrt{2\pi\sigma^2}} \exp\left(-\frac{(t - \tau)^2}{2\sigma^2}\right) \quad (1)$$

To start the iteration, we use the actual parameter values (time at pulse maximum, width of signal at half pulse height, and pulse maximum) of the original waveform.

The averaged time value  $\tau$  of the estimated waveform is used to exploit the temporal form of the received pulses. The averaged range value  $r$  can then easily be determined by

$$r = \frac{\tau c}{2} \quad (2)$$

where  $c$  is the speed of light.

### 3.2 Segmentation

General approaches for segmenting laser range data, as those described by Besl (1988), usually do not take into account the additional information acquired by full waveform processing and therefore have to be expanded upon.

By using waveform processing, we are not only generating a range image, but in fact a whole set of data for each pixel. For the purposes of this paper, the features of particular importance

will be: range for each return pulse, intensity for each return pulse, and number of return pulses. The number of return pulses is used as a clue to region boundaries, while range and intensity further facilitate identifying homogeneous regions inside these boundaries. Without these multiple pulse clues, the region boundaries can not reliably be pinpointed with pixel accuracy. Since the sub-pixel localization scheme works on the intensity of pixels partially covering a surface, this pixel precision is necessary for the accuracy of the resulting edges.

Proceeding from these boundary clues, an iterative region growing algorithm examines the range properties of all pulses in the spatial neighborhood: if the range difference of a pulse and the proofing pulse is below a given threshold, then the pulse is connected and grouped as a new element to this region.

The segmentation leads to a description of image pixels as *region interior* or *region boundary*. The region interior is characterized by single reflections and fills up the region to the boundary. For each homogeneous region found in this manner, the average return pulse power  $P_0$  inside this region is calculated and stored. The region boundary pixels are connected in a 4-neighbor fashion, i.e. each boundary pixel has at least one neighbor in horizontal or vertical direction which also belongs to the boundary.

## 4. BOUNDARY REFINEMENT

To achieve a higher precision for object localization and reconstruction, it is desirable to further refine these measurements (Figure 2a). Standard sub-pixel edge localization approaches use the intensity of grayscale images to obtain improved edge information. The intensity values acquired may form a grayscale image and thus permit the application of these algorithms to our data. But we will go one step further since the full waveform laser data has several advantages over passive optical images for this purpose.

For precise edge localization, it is important to know the properties of the data acquisition unit very well and be able to model the effects of a beam being only partially reflected by a given surface. This modeling will be explained in the first subsection. In the second subsection, we will show how this model enables us to determine the sub-pixel location of an edge in each pixel. The third subsection will examine a straightforward approach to determine edge direction using neighborhood information. Then we will detail our proposed scheme to use the complete edge information to fortify the edge estimate in the fourth subsection. The last subsection will deal with vertices and the problem of their precise localization in the image.

For the purposes of this paper, we will call the measured edge pixels of the image *boundary pixels*, or *corners*, if they do not belong to a straight edge. Furthermore, let the true geometry be denoted by *edges* and *vertices*, to clear up the description of our approach.

### 4.1 Modeling the rasterized edge intensity profile

As shown in the introduction to this Section, it is necessary to be aware of the meaning of the intensity values acquired alongside the range measurements. Therefore we will examine the results of a beam hitting a homogeneous surface perpendicular to the beam propagation direction assuming uniform reflectance for the surface.

An analysis of the spatial beam profile (Jutzi *et al.*, 2002) has shown that it can be approximated by a radially symmetric

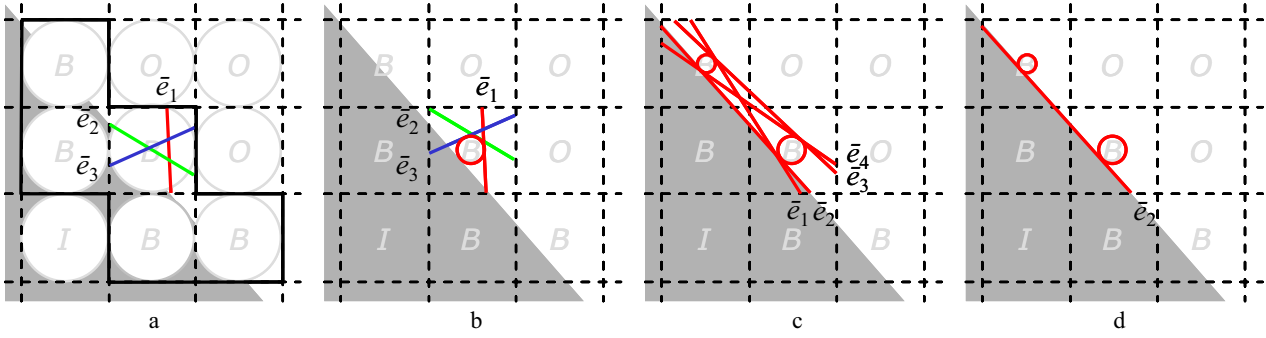


Figure 2. Edge estimation (Pixels labelled *I* are inner region pixels, *O* are outside pixels, and *B* are boundary pixels): a) sample of edges  $\bar{e}_1$ ,  $\bar{e}_2$  and  $\bar{e}_3$ , b) estimated edges by considering the distance from the beam center  $d$ , c) possible edges tangential to two circles, d) final edge by using the signs of  $d_i$

Gaussian distribution for the sake of simplicity. For the case of the beam partially hitting the surface, we assume the object edge to be straight. In reality, this is not a very strong demand, since the edge has to be essentially straight only for the extent of the beam. Furthermore, we let the edge be parallel to the  $y$ -coordinate axis. Because of the radial symmetry of the beam profile, the results can then be generalized to arbitrary edge orientations. If we let  $d$  the distance of the surface edge to the beam center,  $\sigma$  the standard deviation of the beam profile and  $P_0$  the average beam power inside the region (q.v. Section 3.2), we find the reflected beam power to be

$$P_B(d) = \frac{P_0}{\pi\sigma^2} \int_{-\infty}^{\infty} \int_{-\infty}^d e^{-\frac{x^2+y^2}{\sigma^2}} dx dy = \frac{P_0}{\sqrt{\pi\sigma^2}} \int_{-\infty}^d e^{-\frac{x^2}{\sigma^2}} dx \quad (3)$$

This integral can be described by the complementary error function

$$P_B(d) = \frac{P_0}{2} \operatorname{erfc}\left(-\frac{d}{\sigma}\right) \quad (4)$$

Figure 3a shows a plot of the beam intensity versus the edge offset. Here, the grid spacing is  $2f$  and the standard deviation of the Gaussian used to model the beam profile is  $f/3$ .

#### 4.2 Sub-pixel edge localization in each pixel

Looking at a boundary pixel, we can easily acquire the edge distance from the beam center  $d_s$  by inverting the above relationship (using standard numerical procedures) and applying it to the measured return pulse power  $P_B$ . However, it is impossible to estimate the edge orientation using only a single pixel (Figure 2b). Therefore we now have a circle with radius  $d_s$  around the beam center and know that the edge has to be a tangent to this circle (Figure 3b).

To determine the orientation of this tangent, and along with it the orientation of the edge, we have to use neighborhood information to further restrict the edge hypotheses.

#### 4.3 Estimating tangents in 2 neighborhood edge pixels

A very simple approach consists of using a neighborhood boundary pixel to reduce the problem's degrees of freedom. If we have hints that both of these pixels belong to the same straight object edge, we can use their combined information to estimate the edge. We are looking for a line that is tangential to two circles (radii  $d_1$  and  $d_2$ , respectively). This problem generally has four different solutions (Figure 2c), mathematically. From the intensity response, we know which side of the beam center the tangent passes through, since we

actually get a signed result for  $d_1$  and  $d_2$ , corresponding to the measured intensity being smaller or larger than 50% of the intensity inside the region (Figure 3a & b). If the signs of these two radii are different, the correct edge solution is one of the two tangents crossing between the circles, else one of the outer tangents.

From the segmentation step it is already known which side is the inner and which is the outer side of the boundary, i.e. we know where the boundary is connected to the region. Again, watching the signs of  $d_1$  and  $d_2$ , we know which of the two remaining solutions to choose (Figure 2d, in this case both of the signs are negative).

However, this straightforward approach is very sensitive to noisy data, since it does not use an over-determined system of equations. We will be applying our method to urban areas, where we assume much longer edges to be present. This full edge information can be used to gain higher precision results.

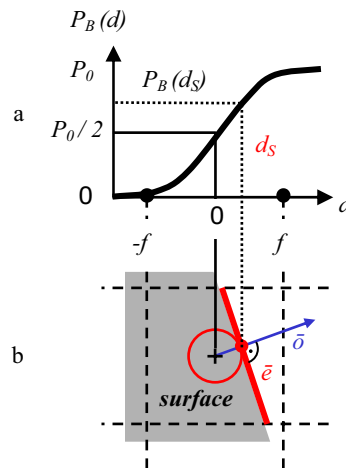


Figure 3. a) Edge  $\bar{e}$  with distance  $d_s$ , b) Integration over the spatial beam profile (the grid spacing is  $2f$ )

#### 4.4 Complete edge localization

To use the complete information available for any given edge, we first have to determine the set of boundary pixels belonging to that edge. In the description of the segmentation algorithm, we already explained how to find region boundaries (Section 3.3). This boundary is transformed into a polygon, at first taking each pixel as a vertex (solid line in Figure 4). If there are any pixels in this list occurring more than once, all of their instances are removed. We do this because we assumed each

pixel to belong to only one edge, therefore mixed pixels are not allowed to appear in our calculation.

This vertex list is then pruned by removing all vertices not significantly affecting the polygon contour. This is achieved by tentatively removing each vertex in turn from the contour (dashed line) and calculating the distance of the new polygon (dotted line) to all boundary pixels along this edge. If the largest of these distances  $g$  is smaller than one half pixel, the vertex is removed permanently. This step is repeated until no more vertices can be removed.

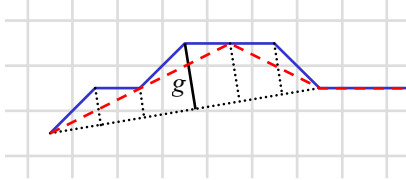


Figure 4. Region boundary simplification

The last polygon found in this fashion is now a pixel-precise estimate of the region boundary, composed of a minimal number of vertices and edges of maximal length. To increase the precision of our estimates for each of these edges, we select the set of all boundary pixels along this edge, leaving out the vertices themselves because of our assumption of pixels fully belonging to straight edges.

For this set of  $k$  points,

$$(\bar{p}_i)_{i \in \{1,2,3,\dots,k\}} \subset \mathcal{R}^2 \quad (5)$$

we calculate the edge distances  $d_i$  from the pixel intensity and solve the optimization problem

$$J = \frac{1}{2k} \sum_{i=1}^k (\bar{n}\bar{p}_i - c - d_i)^2 \quad (6)$$

for the edge normal  $\bar{n}$  and the edge offset to the coordinate origin  $c$ .

As we see, the functional connection between  $P_B$  and  $d$  does not appear in the formula. Therefore the above problem is a fairly standard optimization problem. Going back to the image, if we replace each intensity value  $P_B$  by the associated value  $d$ , Equation 6 corresponds to a standard edge localization problem in grayscale images. However, we now have the advantage of knowing our edge models exactly and can present a finer solution than those typically found for passive imagery. Parameterizing the edge normal  $\bar{n}$  by its direction ( $\bar{n} = (\cos \varphi, \sin \varphi)$ ), we have a simple two-dimensional optimization problem, though it is nonlinear in  $\varphi$ . We solve for  $\varphi$  using the trust region approach by Coleman & Li (1996). The edge offset to the origin  $c$  can then be estimated by

$$\hat{c} = \frac{1}{k} \sum_{i=1}^k (\bar{n}\bar{p}_i - d_i) =: \bar{n}\bar{p} - \bar{d} \quad (7)$$

which is very simple to solve.

#### 4.5 Estimating vertices

Due to the modeling approach, our edge model is correct only for straight edges and incorrect for vertices or curves. Therefore we have been explicitly leaving out corner pixels in the edge localization step. To determine the vertices of the depicted geometry, we calculate the intersections of every pair of neighboring edges.

We chose this approach since the connection of vertex location with the measured intensity is very ambiguous. Furthermore, corners are usually darker and thus more strongly affected by the detector noise. Tying their information in to our optimization problem would complicate matters, remove the independence of neighboring edge localization problems, and does not promise much gain.

## 5. EXPERIMENTAL VALIDATION

To test the algorithms, we created several images with various resolutions, by the method described in Section 2. The example presented here has a size of ten by ten pixels. In all of the images, the solid line is the ground truth geometry used for image generation, whereas the dashed line shows the result of the individual processing steps.

The range image depicted in Figure 5a is actually a range segmentation result, i.e. the white pixels designate returns from the examined surface. Figure 5b shows the intensity measurement at the range of the surface. The image was brightened to enhance the visibility of the overlay lines – the darkest gray actually stands for zero measured intensity.

The boundary segmentation algorithm presented in Section 3.3 results in the boundary polygon shown in Figure 5c. The boundary simplification method (Section 4.4) reduces this polygon to the correct five vertices, resulting in Figure 5d. These two images are typical results using only pixel-precise edge localization (for example, if no intensity information is available).

The next image (Figure 5e) shows the corner and boundary masks used for the sub-pixel edge localization algorithm. The black pixel [3|2] is a boundary pixel, but it was not used for boundary simplification and edge localization, since it belongs to two of our edges (compare Figure 5c). The image in Figure 5f shows the result of the sub-pixel edge localization.

Figure 6a and b show two tests with noisy images. For both of these images, it has been assumed that the proper region boundary pixels can still be extracted from the waveform information. For Figure 6a, Gaussian noise with standard deviation 0.1 has been applied to the image. Figure 6b shows the limits of the algorithm at a noise level of 0.3.

Orientation error [°]	A	B	C	D	E
Noiseless case	0.00	0.64	1.21	0.04	0.00
Noise 0.1	2.33	1.86	0.19	0.13	2.77
Noise 0.3	12.6	0.34	39.7	15.9	1.84

Table 1. Edge orientation errors in degrees; Edge A is the horizontal edge at the top of the image, the remaining edges follow clockwise.

Localization error [pixels]	A	B	C	D	E
Noiseless case	0.09	0.05	0.06	0.05	0.03
Noise 0.1	0.24	0.20	0.13	0.12	0.21
Noise 0.3	0.72	0.30	1.04	0.68	0.09

Table 2. Edge localization errors in pixels; The localization error measures the maximum distance of the vertices of the edge estimate to the straight line extension of the ground truth edge.

The results of the edge localization are very accurate, despite the low resolution. The vertex positions are generally precise up to about a tenth to a twentieth of a pixel. Tables 1 and 2 give a detailed result of the errors acquired for the edges. While the performance of the algorithm degrades with noisy data, it is

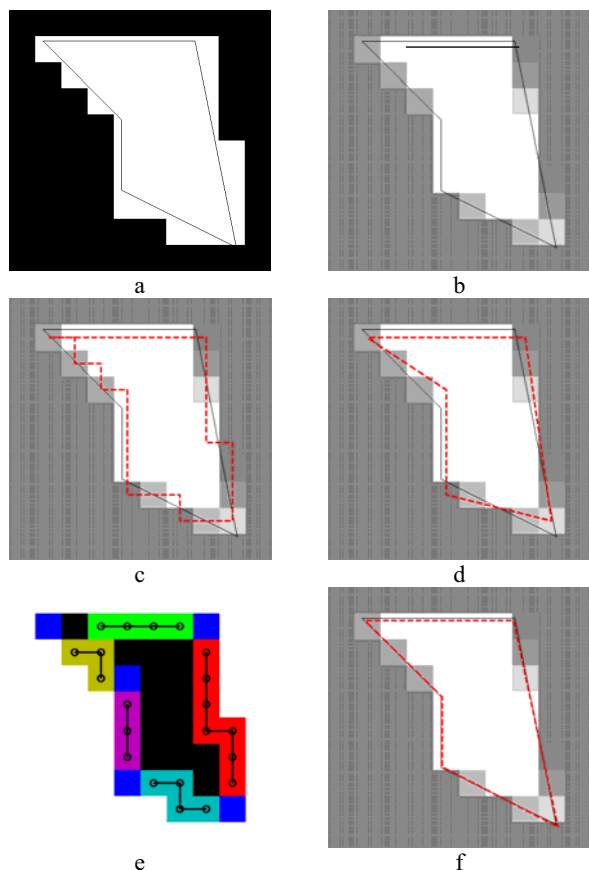


Figure 5. 10x10 source images and results:

- Range image with overlaid ground truth geometry
- Brightened intensity image with ground truth
- Boundary extraction result
- Boundary simplification result (dashed) versus ground truth (solid)
- Boundary and corner masks
- Result of sub-pixel edge localization

evident that longer edges serve to stabilize the results. Edge B, being the longest edge in the test image, gets quite acceptable results even at very high noise levels.

In this work we only considered plane surfaces, fully ignoring the range information except for segmentation purposes. The problems of edge localization in lateral and in range direction are independent of each other and can therefore be tackled separately. Especially in the case of roofs, where the ridge can sometimes not be extracted in the intensity image, a further examination of the geometry in range direction is important.

Also, adjoining surfaces sharing a common edge should be investigated. In this case, we might want to determine one edge using the information from both surfaces instead of two different edges. A typical example for this is a building roof edge, which is usually exactly above an edge between the wall of the building and the ground.

## 6. CONCLUSION

We have presented a scheme to extract the geometry of man-made objects from laser scanning images under the consideration of the intensity value for each received laser pulse. We have shown that using a laser scanner capable of full waveform processing, edge localization precision can be increased by a factor of at least ten. For the actual sub-pixel

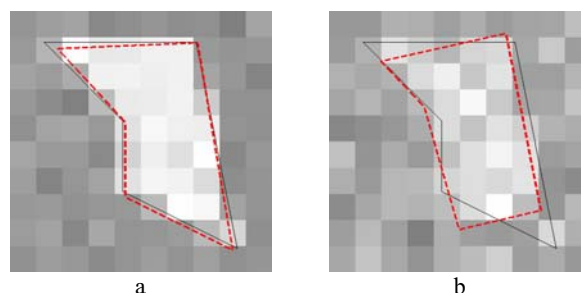


Figure 6. Noisy source images and results:

- Noise standard deviation 0.1
- Noise standard deviation 0.3

localization algorithm the knowledge of a first pulse intensity image would be sufficient. However, the additional information leads to a much more stable segmentation and consequently higher precision edges. The data generation and analysis we carried out are general investigations for a laser system which records the waveform of laser pulses. The method remains to be tested with real data, and expanded to handle more complex geometries (e.g. vehicles, buildings).

## REFERENCES

- Baltsavias EP (1999) Airborne laser scanning: existing systems and firms and other resources. *ISPRS Journal of Photogrammetry & Remote Sensing* 54: 164-198.
- Besl PJ (1988) *Surfaces in Range Image Understanding*. New York: Springer-Verlag.
- Coleman TF, Li Y (1996) An Interior, Trust Region Approach for Nonlinear Minimization Subject to Bounds, *SIAM Journal on Optimization*, Vol. 6, pp.418-445
- Hartley R, Zisserman A (2000) *Multiple View Geometry in Computer Vision*. Proc. Cambridge University Press, Cambridge.
- Hug C, Wehr A (1997) Detecting and identifying topographic objects in laser altimeter data. *ISPRS, International Archives of Photogrammetry & Remote Sensing*, Vol. 32, Part 3-4W2: 19-26.
- Huising EJ, Gomes Pereira LM (1998) Errors and accuracy estimates of laser data acquired by various laser scanning systems for topographic applications. *ISPRS Journal of Photogrammetry & Remote Sensing* 53: 245-261.
- Jutzi B, Eberle B, Stilla U (2002) Estimation and measurement of backscattered signals from pulsed laser radar. In: Serpico SB (ed) (2003) *Image and Signal Processing for Remote Sensing VIII*, SPIE Proc. Vol. 4885: 256-267.
- Jutzi B, Stilla U (2003) Analysis of laser pulses for gaining surface features of urban objects. 2nd GRSS/ISPRS Joint Workshop on Remote Sensing and data fusion on urban areas, URBAN 2003: 13-17.
- Jutzi B, Stilla U (2004) Extraction of features from objects in urban areas using space-time analysis of recorded laser pulses. In: Altan MO (ed) *International Archives of Photogrammetry and Remote Sensing*. Vol. 35, Part B2, 1-6.
- Maas HG (2001) The suitability of airborne laser scanner data for automatic 3D object reconstruction. In: Baltsavias EP, Gruen A, Van Gool L (eds) *Automatic Extraction of Man-Made Objects From Aerial and Space Images (III)*, Lisse: Balkema.
- Vosselman G (2002) On estimation of planimetric offsets in laser altimetry data. Vol. XXXIV, *International Archives of Photogrammetry and Remote Sensing*: 375-380.
- Wagner W, Ullrich A, Melzer T, Briese C, Kraus K (2004) From single-pulse to full-waveform airborne laser scanners: Potential and practical challenges. In: Altan MO (ed) *International Archives of Photogrammetry and Remote Sensing*. Vol 35, Part B3, 201-206.
- Wehr A, Lohr U (1999) Airborne laser scanning – an introduction and overview. *ISPRS Journal of Photogrammetry & Remote Sensing* 54: 68-82.